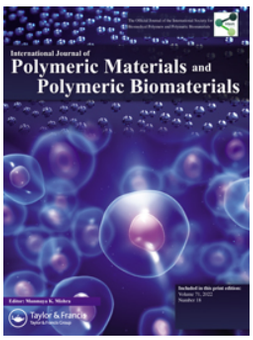

International Journal of Polymeric Materials and Polymeric Biomaterials

ISSN: (Print) (Online) Journal homepage: https://www.tandfonline.com/loi/gpom20

Magnetic polycaprolactone microspheres: drug encapsulation and control

Nesrine Abdelrehim El Gohary, Abdelrahman Mahmoud, Mohamed Ashraf Nazmy, Rami Zaabalawi, Loaa El Zahar, Islam S. M. Khalil & Mohamed E. Mitwally

To cite this article: Nesrine Abdelrehim El Gohary, Abdelrahman Mahmoud, Mohamed Ashraf Nazmy, Rami Zaabalawi, Loaa El Zahar, Islam S. M. Khalil & Mohamed E. Mitwally (2022): Magnetic polycaprolactone microspheres: drug encapsulation and control, International Journal of Polymeric Materials and Polymeric Biomaterials, DOI: 10.1080/00914037.2022.2132248

To link to this article: https://doi.org/10.1080/00914037.2022.2132248

INTERNATIONAL JOURNAL OF POLYMERIC MATERIALS AND POLYMERIC BIOMATERIALS
https://doi.org/10.1080/00914037.2022.2132248

Magnetic polycaprolactone microspheres: drug encapsulation and control

Nesrine Abdelrehim El Gohary[a]*, Abdelrahman Mahmoud[b]*, Mohamed Ashraf Nazmy[c], Rami Zaabalawi[c], Loaa El Zahar[d], Islam S. M. Khalil[e], and Mohamed E. Mitwally[b]

[a]Pharmaceutical Chemistry Department, Faculty of Pharmacy and Biotechnology, German University in Cairo, Cairo, Egypt; [b]Materials Engineering Department, Faculty of Engineering and Materials Science, German University in Cairo, Cairo, Egypt; [c]Faculty of Pharmacy and Biotechnology, German University in Cairo, Cairo, Egypt; [d]Faculty of Media Engineering and Technology, German University in Cairo, Cairo, Egypt; [e]Department of Biomechanical Engineering, University of Twente, Enschede, the Netherlands

ABSTRACT

Targeted drug delivery (TDD) systems have several advantages, especially with drugs having toxic side effects such as lornoxicam (LX) which shows high hepatotoxicity and nephrotoxicity, especially with long-term use. This work represents an attempt to control magnetic microspheres encapsulating LX and magnetite nanoparticles (MNPs) for potential targeted drug delivery of LX. Superparamagnetic nanoparticles were fabricated via the co-precipitation method and together with LX were encapsulated into polycaprolactone (PCL) microspheres through an oil-in-water (O/W) emulsion solvent evaporation method. The effects of changing the amount of drug, MNPs, and volume of the aqueous phase were investigated by preparing several microsphere formulations. Increasing the amount of encapsulated MNPs increased the magnetization of the microspheres without affecting the morphology. Doubling the volume of the aqueous phase resulted in a higher encapsulation efficiency and drug loading; 83.9% and 10.7%, respectively, while increasing the amount of drug had a negative effect on both drug loading and encapsulation efficiency. Drug release from the microspheres was successfully achieved and showed a biphasic nature. A system of four planar coils was then used to magnetically control the movement of a cluster of capsules in a glycerin medium, as a simulation for the targeting process. The microspheres were successfully controlled to move in a U-turn path with sharp corners demonstrating their potential for TDD applications.

GRAPHICAL ABSTRACT

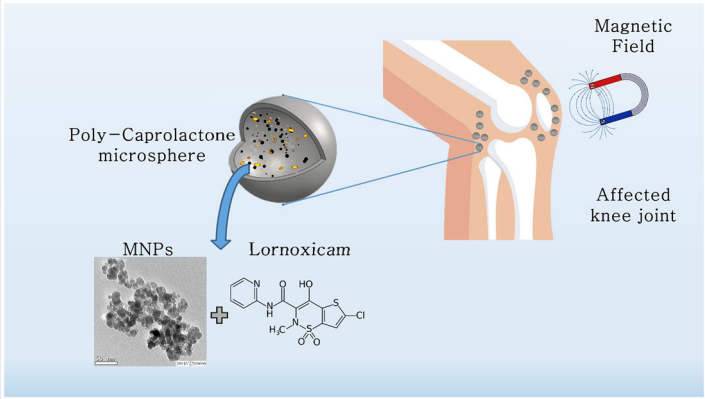

Abbreviations: TDD: targeted drug delivery; LX: lornoxicam; MNPs: magnetite nanoparticles; PCL: polycaprolactone; O/W: oil in water; *v/v*: volume per volume; *w/v*: weight per volume; NSAIDs: non-steroidal anti-inflammatory drugs; PLA: polylactide; RES: reticular endothelial system; VSM: vibratory sample magnetometer; FTIR: Fourier transform infrared; DCM: dichloromethane; NODCAR: National Organization of Drug Control and Research; PVA: polyvinyl alcohol; UPW: ultra-pure water; XRD: X-ray diffractometer; HRTEM: high resolution transmission electron microscope; SEM: scanning electron microscope; EDS: energy dispersive spectroscopy; BET: Brunauer–Emmett–Teller; PBS: phosphate buffer saline

ARTICLE HISTORY

Received 18 July 2022
Accepted 30 September 2022

KEYWORDS

Drug release; lornoxicam; magnetic control; magnetite; polycaprolactone microspheres; targeted drug delivery

CONTACT Nesrine Abdelrehim El Gohary nesrine.elgohary@guc.edu.eg Pharmaceutical Chemistry Department, German University in Cairo, Cairo, Egypt.
*Both Nesrine Abdelrehim El Gohary and Abdelrahman Mahmoud contributed equally to the work.

Supplemental data for this article can be accessed online at https://doi.org/10.1080/00914037.2022.2132248.

1. Introduction

Non-steroidal anti-inflammatory drugs (NSAIDs) are commonly used to alleviate acute or chronic inflammation such as in the case of rheumatoid arthritis and osteoarthritis. In the case of chronic diseases, long-term treatment is required. Long-term treatments are associated with an increased risk of gastrointestinal, liver, cardiac, and renal toxicities[1]. Loading the drugs into a carrier system offers increased drug stability in plasma, enhanced tissue penetration, and minimizes nonspecific distribution of the drug, thus avoiding associated toxicities and allowing for long-term usage[2,3]. Drug carriers are commonly fabricated from either biocompatible and biodegradable polymers or biogenic materials. Biodegradable polymers used for drug delivery include hydrogels, polycaprolactone (PCL), and polylactide (PLA) while examples of biogenic drug carriers include human hair, squid-derived proteins, and bovine sperm[4–9].

Targeting drug carrier vehicles to the site of action offers localization of the drug at specific locations, thus avoiding the systemic side effects the drug could cause and increasing the efficiency of treatment. Moreover, improved patient compliance is achieved via reducing the drug dose needed[10]. As targeting moieties of drug carriers; antigen–antibody reaction, pH, temperature, and magnetic field have been widely used[11–15]. In addition, different external stimuli have been exploited to improve drug delivery as ultrasound-assisted drug delivery, light-responsive drug delivery, and chemically-triggered drug delivery[16–18]. Motion control of drug carriers on the other hand has been demonstrated using light, ultrasound, electric fields, and magnetic fields[19–22]. Magnetic fields offer several advantages in controlling drug carriers. Magnetic control over drug carriers requires low-strength fields which are harmless to human cells and tissues. Moreover, electromagnetic and magnetic manipulation systems have the capability to produce controlled magnetic fields and can be scaled to the size of *in vivo* applications. To date, the most promising manipulation system involves the use of a rotating permanent magnet fixed to the end-effector of a robotic manipulator to provide an open configuration and relatively large workspace[23]. Another open configuration permanent magnet-based manipulation system was used by Neidert et al. who demonstrated the first *in vivo* motion control and localization of a tumbling microrobot using rotating magnetic fields and ultrasound images, respectively[24]. An electromagnet-based manipulation system with a large workspace was also successful in controlling a tetherless magnetic drug carrier during *in vitro* retinal procedures with a potential for drug delivery[25].

In the case of magnetic drug targeting, magnetic nanoparticles (MNPs), such as magnetite and maghemite, could be suitably functionalized and loaded directly with the drug either by conjugation reactions or strong physical adhesion of the drug to the particles. However, there are several limitations to this approach. Premature or fast drug release may occur, the loading capacity is relatively low and it is highly likely that the particles will be up-taken by the reticular endothelial system (RES) before reaching the site of action[11,26,27]. An alternative pathway to avoid such problems is loading both the drug and magnetic particles on polymeric vehicles. This approach combines the advantages of drug carrier systems and magnetic targeting. This combination has been previously applied for different drugs that can lead to toxic side effects and require localization at the site of action such as the anti-cancer drugs; doxorubicin[28] and 5-fluorouracil[5] A few studies have adopted this approach for chronic diseases such as rheumatoid arthritis and osteoarthritis[29–32] where most studies related to magnetic drug targeting are focused on the treatment of cancer.

Lornoxicam (LX), an NSAID of the oxicam class is a yellow crystalline solid used in the treatment of osteoarthritis and rheumatoid arthritis with an analgesic effect comparable to that of opioids[1]. LX exerts its anti-inflammatory and analgesic activities through its inhibitory action on COX-1 and COX-2 enzymes and therefore inhibits prostaglandin and thromboxane synthesis. Its short half-life (3–5 h) makes the development of sustained release formulations highly beneficial. Moreover, LX shows hepatotoxicity and nephrotoxicity which are pronounced with long-term use, leading to potential toxic effects[33]. Accordingly, using a magnetic polymeric drug carrier vehicle to direct LX to the site of action would eliminate undesirable side effects and could also allow for sustained release of the drug.

In this study, LX was encapsulated along with Fe_3O_4 as MNPs in PCL microspheres through an (O/W) emulsion solvent evaporation method. The microspheres were characterized in terms of shape and size using electron microscopy and in terms of magnetism using a vibratory sample magnetometer (VSM). Fourier transform infrared (FTIR) analysis was used to confirm the composition. Drug loading, encapsulation efficiency, and *in vitro* drug release profile were determined. The ability to magnetically control the microspheres was also investigated using a system consisting of four electromagnetic coils in a planar configuration.

2. Materials and methods

2.1. Materials

LX standard was supplied by the National Organization of Drug Control and Research (NODCAR). To fabricate the drug-carrying microspheres, high molecular weight polycaprolactone (PCL) (Molecular weight = 70,000–90,000 g/mol; Sigma–Aldrich, Germany) was used. Other chemicals purchased from Sigma–Aldrich were polyvinyl alcohol (PVA), $FeSO_4{\cdot}7H_2O$, $FeCl_3{\cdot}6H_2O$, oleic acid, dichloromethane (DCM), and ammonia solution (33%). For the dispersing phase, ultra-pure water (UPW) purified in purelab UHQ (ELGA) was used throughout this work.

2.2. Magnetic nanoparticles preparation and characterization

MNPs coated with oleic acid were prepared via chemical co-precipitation using a method adapted with modifications

Table 1. Microspheres preparations.

Formulation code	Drug (mg)	PCL (mg)	MNPs (mg)	2% *w/v* PVA solution (mL)
F1	50	250	60	20
F2	50	250	90	20
F3	50	250	90	40
F4	80	250	90	40
F0		250	90	40

from Liang et al.[34]. This method was chosen due to its simplicity, efficiency, and high yield[35]. Oleic acid was chosen as a surfactant in order to increase the hydrophobicity of the particles which facilitates their dispersion in organic media thus decreasing agglomeration and increasing the stability of MNPs[36].

Briefly, $FeSO_4 \cdot 7H_2O$ and $FeCl_3 \cdot 6H_2O$ in a molar ratio of 1:2 were dissolved in UPW under the flow of N_2 gas. This was followed by the dropwise addition of 20 mL of concentrated ammonia solution (33%) at 80 °C under vigorous stirring. After which, 4 mL of oleic acid were added to the resultant MNPs, followed by stirring for 30 min at 80 °C. Finally, the MNPs were washed with UPW followed by drying.

The structure of the nanoparticles was investigated using X'Pert^3 Powder X-ray diffractometer (XRD) equipped with a Cu-Kα source. The size and morphology of the nanoparticles were characterized using a JEOL JEM-2100 high-resolution transmission electron microscope (HRTEM) operated at 200 kV. The superparamagnetic behavior of the fabricated MNPs was checked using a Lake Shore 7410 vibrating sample magnetometer (VSM). FTIR analysis recorded in the range of 4,000–400 cm^{-1} using Nicolet Avatar 380 spectrometer (Germany) was also used to characterize the synthesized MNPs.

2.3. Polycaprolactone microspheres preparation and characterization

The magnetic microspheres containing LX were prepared by the O/W emulsion solvent evaporation technique[37]. The organic phase was prepared by dissolving PCL in 10 mL DCM, followed by the addition of LX and MNPs, and then the mixture was sonicated for 10 min. The aqueous phase was prepared by dissolving PVA 2% *w/v*, where two different volumes of the aqueous phase were investigated; 20 and 40 mL. The organic phase was then added to the aqueous phase drop by drop under probe sonication in a time span of 15 min. The mixture was then left to shake in an orbital shaker for 3 h to allow solvent evaporation. Finally, the microspheres were left to dry for further use. Four different formulations (F1, F2, F3, and F4) were synthesized as shown in Table 1. A blank formulation (F0) was prepared in the same way as F3 and F4 but without including LX in the preparation.

The external and internal morphology of the microspheres were characterized by a Quanta FEG250 Scanning electron microscope (SEM) and JEOL, JEM-2100 HRTEM. Energy dispersive spectroscopy (EDS) was performed to determine the composition of the microspheres. The magnetic behavior on the other hand was evaluated by Lake Shore 7410 VSM. Brunauer–Emmett–Teller (BET) method was employed to calculate the specific surface areas, while pore size and volume were calculated using Barrett–Joyner–Halenda (BJH) method via Quantachrome INSTRUMENTS (USA).

2.4. Determination of encapsulation efficiency and drug loading

The amount of drug entrapped in F3 and F4 microspheres was calculated by dissolving 10 mg of dry microspheres into 10 mL 50% (*v/v*) formic acid. The amount of drug was calculated by analyzing the solution using UV-Visible Spectrophotometer (Jasco V630) at 375 nm (λ_{max}) of LX. F0 was used as blank in the calculations. The encapsulation efficiency and drug loading percentages were calculated using Equations 1 and 2, respectively, as follows:

$$\text{Encapsulation efficiency } \% = \frac{\text{Experimental drug content}}{\text{Theoritical drug content}} \times 100 \quad (1)$$

$$\text{Drug loading } \% = \frac{\text{Experimental drug weight}}{\text{Experimental capsule weight}} \times 100 \quad (2)$$

2.5. In vitro drug release studies

In vitro release studies for formulated magnetic microspheres were performed in phosphate buffer saline (PBS), pH 7.4. Ten mg of F3 microspheres were suspended in 15 mL of PBS in a rotating water bath at 37 °C. At predetermined time intervals, 1 mL of the sample solution was withdrawn and replaced with the same volume of fresh buffer. The amount of drug released in media was determined by measuring the absorbance using a UV-Visible Spectrophotometer at 375 nm. The experiment was done in duplicates.

To study the drug release kinetics and mechanism, the cumulative release data obtained from *in vitro* release studies were fitted to various models; zero order (Q vs. t), first order ($\text{Log}(Q_0 - Q)$ vs. t), and Higuchi (Q vs. $t^{1/2}$). Here Q represents the cumulative percentage of drugs released in time t and $(Q_0 - Q)$ is the cumulative percentage of drugs remaining after time t. The nature of the release of the drug from the formulated magnetic microspheres was explained based on the correlation coefficients obtained from the plots of the kinetic models. The model with the highest correlation coefficient close to unity was taken as the appropriate model.

2.6. Magnetic control of microspheres

A system consisting of four electromagnetic coils in one horizontal plane shown in Figure 1 was used to control the movement of a cluster of microspheres, shown in the inset

figure, in an open loop fashion via a joystick (Logitech-Extreme 3D Pro). The cluster of microspheres (F3) was controlled via external magnetic fields generated by the four electromagnets in a glycerin medium. The control algorithm uses a magnetic field strength of approximately 42 mT. The magnetic field direction changes when the joystick reference position changes. The magnetic field is measured using a calibrated three-axis Hall magnetometer (Sentron AG, Digital Teslameter 3MS1-A2D3-2-2T, Switzerland) as shown in Figure 1.

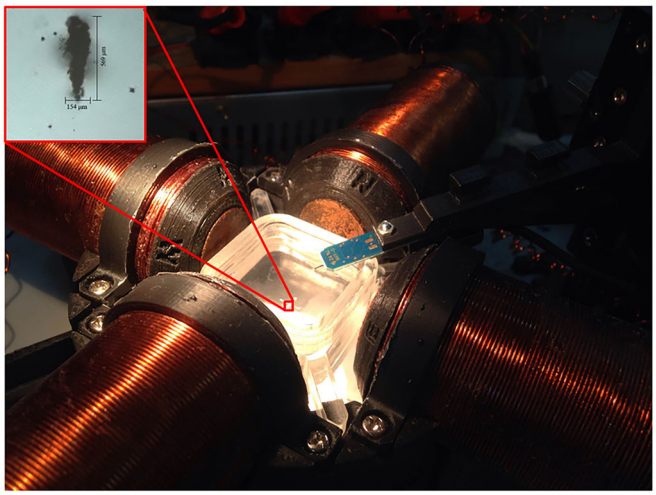

Figure 1. Four planar coil system for magnetic targeting with the inset showing the cluster of microspheres under investigation. A magnetometer is used to measure the magnetic field strength.

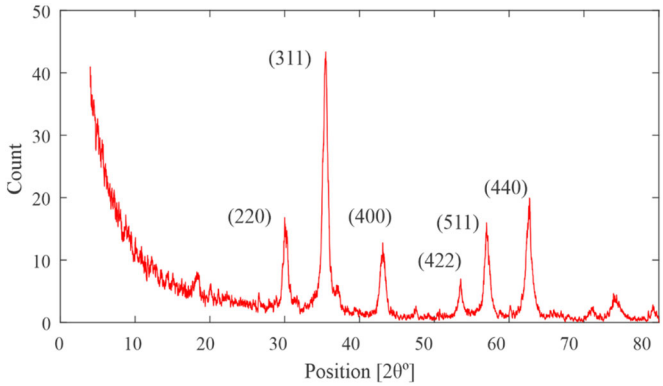

Figure 2. X-ray diffraction pattern of synthesized MNPs showing the different planes to which the peaks correspond.

2.7. Statistical analysis

The results of drug loading and encapsulation efficiency were expressed as mean ± standard deviations. Statistical significance was assessed with one-way ANOVA (Tukey–Kramer multiple comparisons test) by employing Graph Pad Instat (Graph Pad Software Inc., San Diego, California USA). The samples were considered significantly different when $p < 0.05$.

3. Results

In this paper, scalars are denoted by standard font (e.g., V), and vectors are denoted by capital bold font (e.g., $\mathbf{F}$).

3.1. Magnetic nanoparticles characterization

Structural investigation of MNPs via XRD showed the diffraction spectrum in Figure 2. The diffraction peaks were matching with reference peaks of Fe_3O_4 according to JCPDS card No. 00-019-062. This is indicated by the (220), (311), (400), (422), (511), and (440) characteristic peaks of Fe_3O_4 with the (311) peak having the highest intensity and occurring at $2\theta = 35.3°$.

TEM image (Figure 3A) of MNPs shows that they are monodisperse, nearly spherical in shape with a size range between 20 nm and 50 nm.

The magnetic behavior of MNPs tested at room temperature using VSM showed a magnetization saturation (M_s) value of 79.6 emu/g as shown in Figure 4. The MNPs

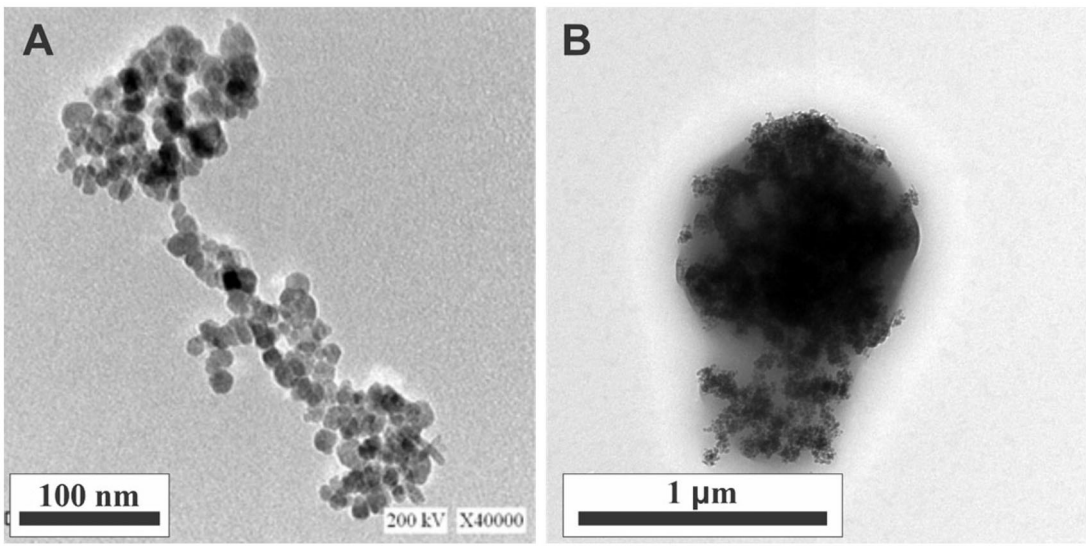

Figure 3. TEM images of (A) MNPs and (B) F3 microsphere.

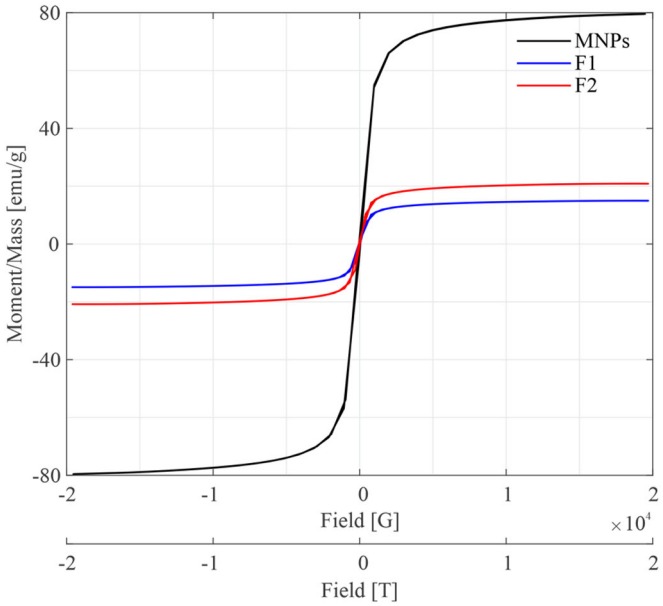

Figure 4. VSM data for MNPs, F1 and F2.

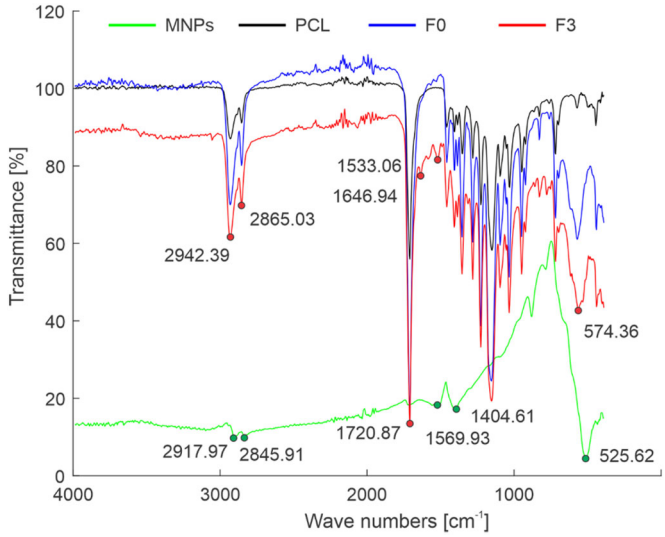

Figure 5. FTIR spectra in the range of 4,000–400 cm^{-1} for MNPs, PCL, F0, and F3.

showed small hysteresis and nearly had no remanence and low coercivity.

FTIR analysis in the range of 4,000–400 cm^{-1} (Figure 5) revealed symmetrical and asymmetrical C–H stretching vibration peaks of oleic acid at 2,846 and 2,918 cm^{-1}, respectively. The bands at 1,569 and 1,404 cm^{-1} are attributed to $-COO^{-}$ stretching vibration. The peak at 526 cm^{-1} is attributed to Fe–O stretching vibration.

3.2. Polycaprolactone microspheres characterization

Four different formulations of microspheres were prepared and characterized; F1, F2, F3, and F4. In F1 and F2 formulations, the amount of magnetite was increased from 60 to 90 mg, and all other parameters such as the amount of LX, PCL, and volume of PVA solution were kept constant as indicated in Table 1. The SEM images of F1 and F2, Figures 6A and 6B, respectively, revealed that microspheres were smooth and poly-disperse having a size ranging between 800 and 2,000 nm. The images also revealed that the microspheres were not well separated.

VSM analysis (Figure 4) revealed a high reduction in magnetization values in comparison to MNPs that had a M_s value of 79.6 emu/g. F2 prepared with 90 mg MNPs showed a higher M_s value (20.9 emu/g) compared to the *Ms* value (15.0 emu/g) of F1 which was prepared with 60 mg MNPs. Thus, it was decided in the following formulations to keep the amount of MNPs at 90 mg.

F3 was prepared similarly to F2; the only difference was that the volume of the aqueous phase was doubled while keeping the percentage of PVA at 2% *w/v*. SEM image (Figure 6C) revealed that the microspheres of F3 were better separated compared to the heavily agglomerated F2 microspheres. The F3 microspheres were smooth with an average size of 1,500 nm.

F4 was prepared similarly to F3; the only difference was that the amount of LX was increased to 80 mg instead of 50 mg. SEM image of F4 (Figure 6D) was similar to F3. The microspheres were smooth, separated, and had an average size of 1,600 nm. F0 blank microspheres prepared similarly to F3 and F4 without adding LX revealed also similar morphology (Figure 6E).

TEM was used to visualize the internal structure of the microspheres. Figure 3B confirmed the encapsulation of MNPs in the microsphere body.

F3 was further characterized using BET and BJH analysis; the results revealed that the microspheres had an average surface area of 7.61 m^2g^{-1}, average pore volume of 0.02 cc g^{-1}, and pore diameter of 3.38 nm.

FTIR in the range of 4,000–400 cm^{-1} was recorded for F3, F0, and pure PCL (Figure 5). Bands appearing at 1,721, 2,865, and 2,942 cm^{-1} in pure PCL, F3, and F0, are assigned to C = O stretching of the ester carbonyl group and symmetric and asymmetric CH_2 stretching vibrations of PCL matrix, respectively[9]. The band at 574.36 present in F3 and F0 is attributed to Fe–O stretching vibration. Two additional bands at 1,647 and 1,533 cm^{-1} are seen in the F3 spectrum but not in the F0 spectrum. The 1,647 and 1,533 cm^{-1} bands correspond to the C = O stretching and N–H bending vibration of LX, respectively[38].

EDS analysis was performed for F3, F4, and F0 microspheres. The results are presented in Figure 7. Carbon and Oxygen peaks are observed in all spectra (Figures 7A, 7B, and 7C), this could be attributed to PCL structure. A peak for Iron was also observed in all spectra while a peak for Nitrogen was only observed in EDS of F3 and F4 and not in EDS of blank formulation (F0).

3.3. Drug loading and encapsulation efficiency

The results of drug loading and encapsulation efficiency for F2, F3, and F4 are shown in Table 2. The results reveal that when the volume of the aqueous phase was doubled in the preparation, both the drug loading content and the encapsulation efficiency increased. This can be seen in Table 2

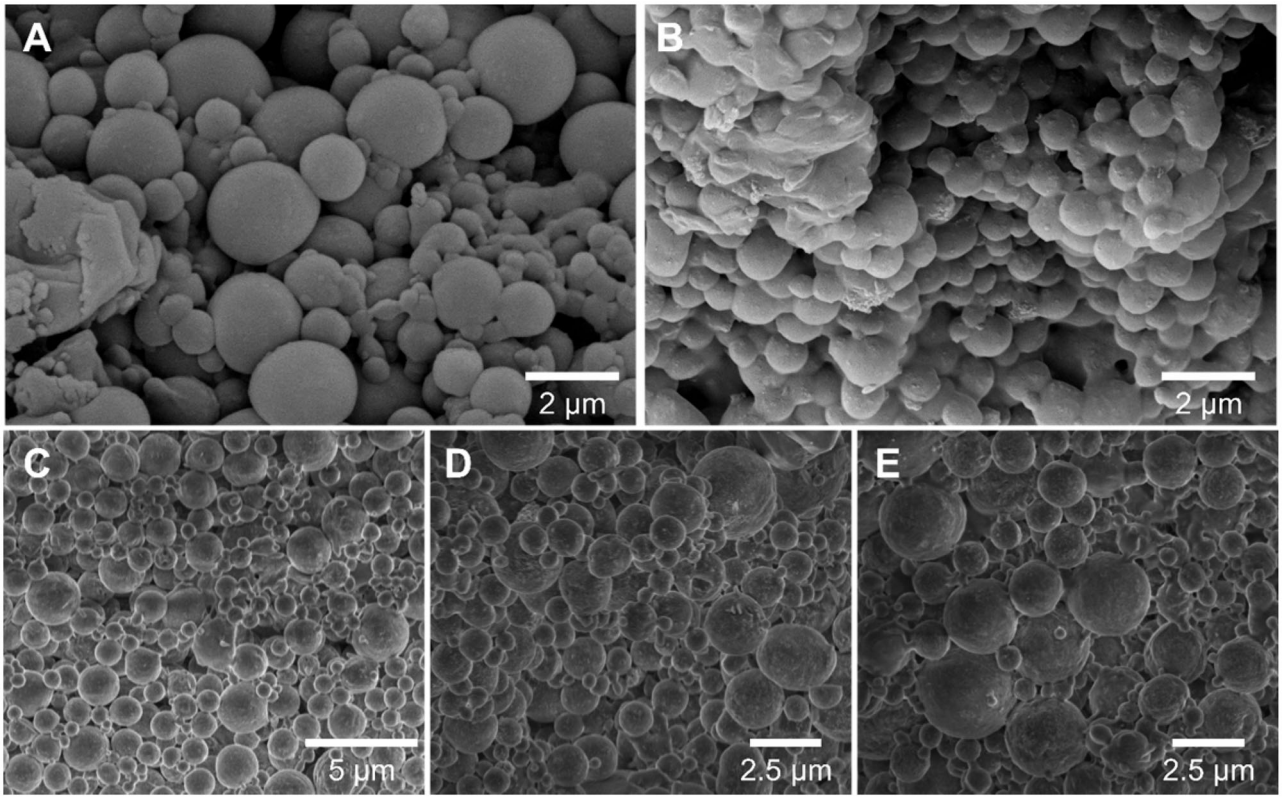

Figure 6. SEM images of F1 (A), F2 (B), F3 (C), F4 (D), and F0 (E).

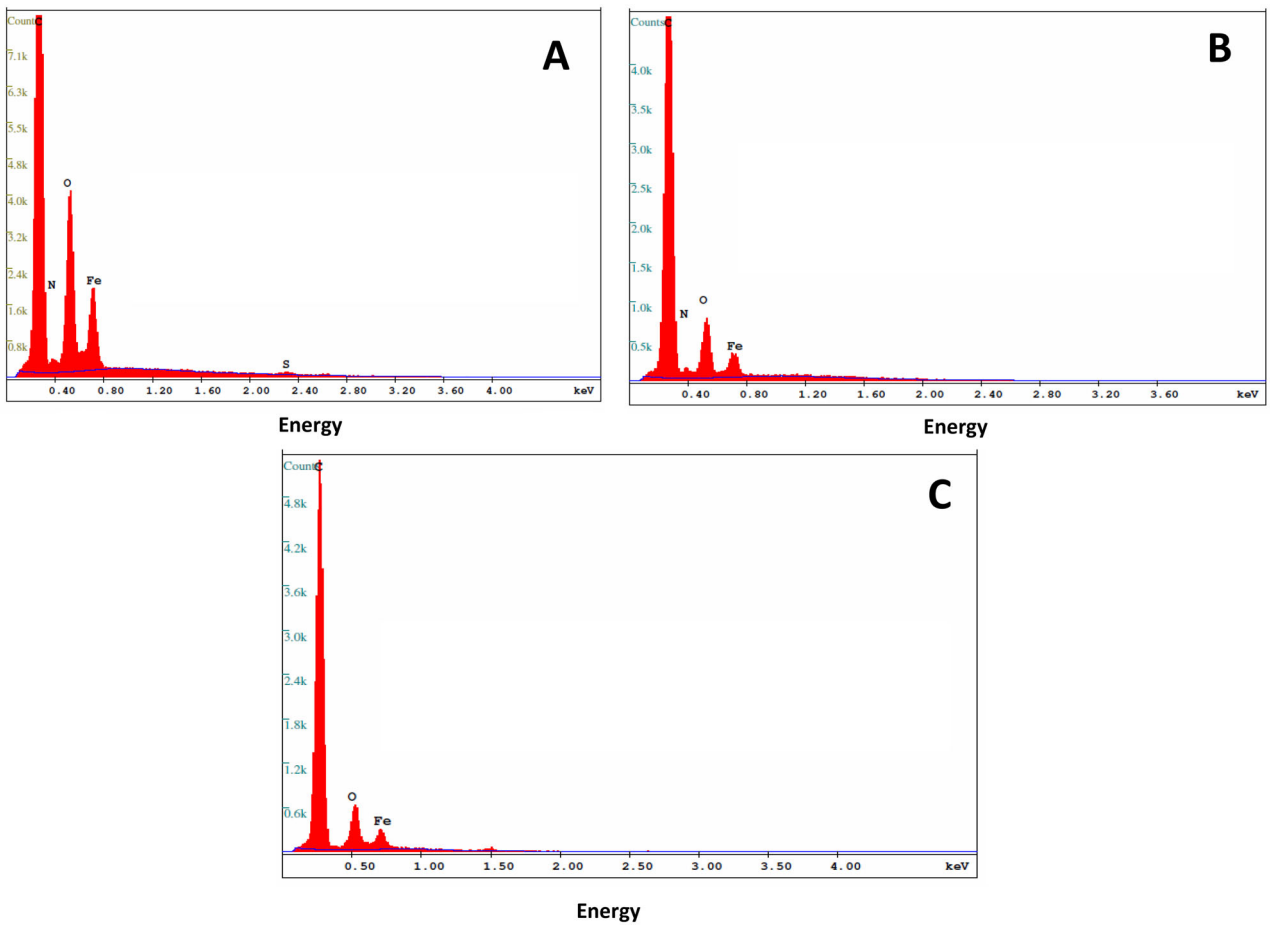

Figure 7. EDS analysis of microsphere fabricated using formulas; F3 (A), F4 (B), and F0 (C).

Table 2. Results of drug loading and encapsulation efficiency.

Formulation number	Drug loading (% ± SD)*	Encapsulation efficiency (% ± SD)
F2	4.8 ± 0.21	37.5 ± 0.47
F3	10.7 ± 0.04	83.9 ± 0.36
F4	8.8 ± 0.35	46.5 ± 1.83

*Mean ± SD of three determinations.

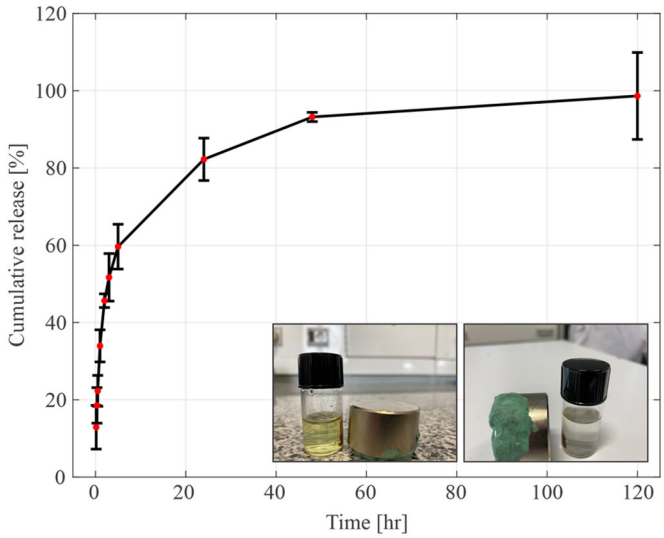

Figure 8. Release profile of LX from F3. Inset figures show the microspheres initially incubated in PBS (right inset) and after 5 days of release (left inset), the yellow color of LX is apparent in the release media.

showing F3 and F4 having higher average drug loading percentages and higher average encapsulation efficiency compared to F2. However, increasing the amount of drug in F4 did not cause an increase in either the drug loading or the encapsulation efficiency, rather, it had a negative effect on both. It was observed during the preparation of F4 that not all of the 80 mg LX added to F4 was completely dissolved in DCM. The highest drug loading (10.7%) and encapsulation efficiency (83.9%) was obtained for F3 and thus it was chosen to experiment with the release profile of the drug from the microspheres. The statistical analysis showed that there was a significant difference in drug loading and encapsulation efficiency between different formulations ($p < 0.05$).

3.4. In vitro drug release studies

The release profile of LX from F3 microspheres was studied in PBS (pH 7.4) at 37 °C. It is evident from the release profile shown in Figure 8 that the drug exhibits a biphasic release. First, there is a fast release of almost 59.6% of the drug content during the first 5 h followed by a sustained slower release of the drug during the subsequent hours. The remaining drug content was released slowly over a period of 5 days where the entrapped drug slowly diffuses out into the release medium.

The kinetics of the drug release were examined using various models. The two phases of drug release, fast release during the first 5 h and slow release during the subsequent hours, were each studied independently using the various kinetics models. Results are shown in Table 3. The model with the correlation coefficient closest to unity was chosen as the optimum model to describe the release kinetics. For the fast release phase, the Higuchi model best describes the release which indicates that at the beginning the release is diffusion controlled. For the slow release phase; first-order kinetics best describes the release.

Table 3. Kinetics of LX release from the microspheres.

Model	Correlation coefficient* R^2	Correlation coefficient** R^2
Zero order	0.8826	0.7925
First order	0.9369	0.9816
Higuchi	0.9751	0.8624

*Fast release phase; **Slow release phase.

3.5. Magnetic control of microspheres

The microsphere cluster showed direction control in response to applied external magnetic fields. The cluster of microspheres had an elliptical shape with a length of 569 µm and a width of 154 µm as shown in the inset of Figure 1. Open loop control was performed inside a glycerin medium. The glycerin medium having a density (ρ) of 1,260 kg/m^3 and dynamic viscosity (μ) of 0.95 Pa s ensures that Reynold's number ($Re = \frac{\rho u L}{\mu}$) is well within the order of 10^{-6}, indicating laminar flow, where u and L are the velocity and length of the cluster, respectively. Figure 9 shows the location of the cluster at different times along a U-turn path with sharp corners under open loop control. The cluster travelled a total distance of 1,808 µm along the U-turn path in a time interval of 35 s. Accordingly, the average swimming speed of the cluster is calculated to be 51.6 µm/s which is about 0.09 body length per second. A supplementary video is provided for the directional control along a *U*-turn path with sharp corners.

4. Discussion

Fabricated MNPs showed comparable magnetic behavior to that reported in the literature for MNPs fabricated via co-precipitation chemical methods in terms of the M_s value measured by VSM. Furthermore, the low coercivity value coupled with an M_s value of 79.6 emu/g confirms the superparamagnetic behavior of the MNPs nanoparticles[4,34,39]. The size range of the MNPs observed via TEM is also comparable to reported sizes in the literature[4,34,39,40]. Such size range is crucial in the encapsulation of MNPs in PCL microspheres without having a significant effect on the size distribution of the microspheres. TEM also reveals that MNPs tend to aggregate due to their high surface area-to-volume ratio. The XRD results on the other hand revealed that no other iron oxide phases such as Fe_2O_3 were significantly present indicating no oxidation occurring during the fabrication process. FTIR results revealed the complex formation between iron atoms and the carboxylate groups of oleic acid, thus, confirming the attachment of oleic acid on the surface of MNPs. This can be indicated by the presence

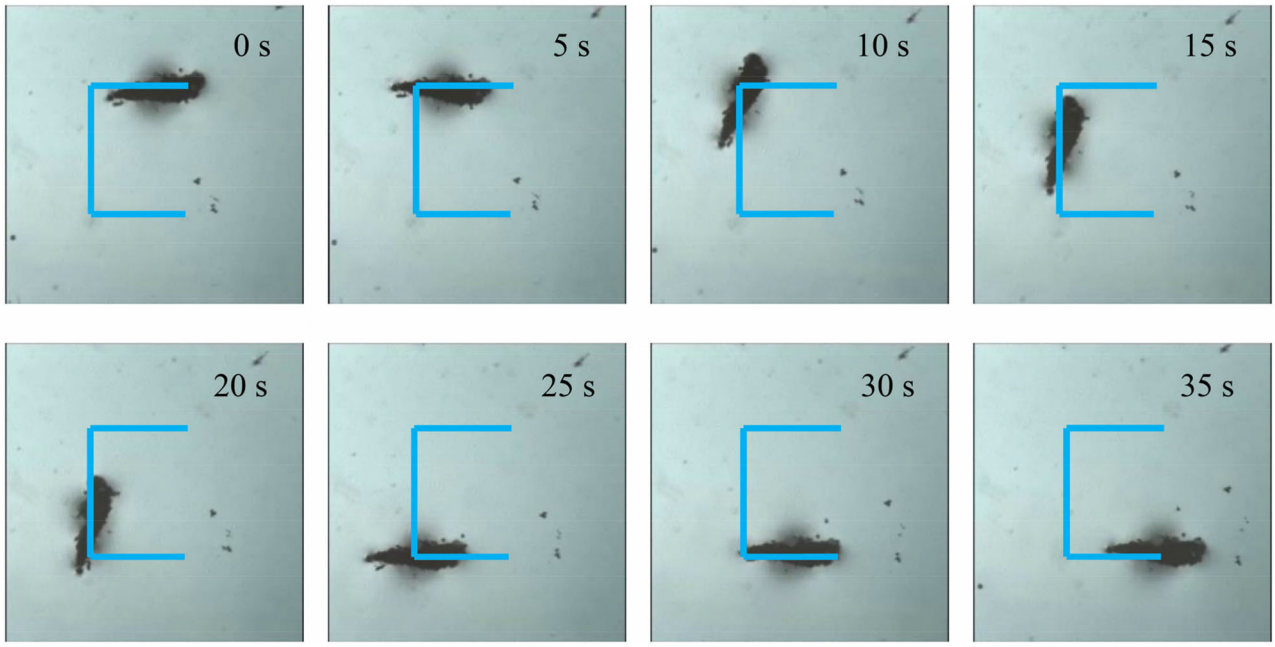

Figure 9. Open loop control on the microspheres cluster (F3) in a U-turn path with sharp corners showing the cluster location at different times.

of the bands at 1,569 and 1,404 cm^{-1} attributed to $-COO^-$ stretching vibration[40,41].

Magnetic PCL microspheres were prepared via the O/W emulsion solvent evaporation technique. This method was chosen as it is a simple economic method having parameters that could be easily controlled and optimized. In this work, three parameters during microsphere preparation were optimized; the amount of magnetite, the amount of drug, and the volume ratio of the aqueous to the organic phase. The increase in the amount of MNPs added during fabrication from 60 to 90 mg resulted in a higher magnetization saturation. Thus, it could be concluded that on increasing the amount of MNPs in the preparation, more MNPs were successfully encapsulated in the microspheres. No, further attempts to increase the amount of MNPs beyond 90 mg were conducted as the microspheres showed excellent direction control in response to applied external magnetic fields. On doubling the volume of the aqueous phase, it was found that microspheres were more defined, more separated, and less entangled with each other, thus, the increase in the volume of the aqueous phase had a positive effect on the preparation process, this most probably could be attributed to the organic phase droplets formed during the emulsion process possessing a bigger volume to spread in, thus, positively affecting the final morphology of microspheres. Moreover, both the drug loading and encapsulation efficiency were significantly increased by doubling the volume of the aqueous phase. It has been previously reported that an increase in the volume of the continuous phase increases the encapsulation efficiency, where a large volume of the continuous phase leads to a fast solidification process as a result of providing a high concentration gradient of the organic solvent across the phase boundary by diluting the solvent[42]. The effect of increasing the drug content during the preparation of the microspheres had no effect on the final morphology of the microspheres but rather had a negative effect on encapsulation efficiency, this could be attributed to the high concentration gradient resulting in the drug diffusing out of the polymer/solvent droplets to the external processing medium[43].

The successful incorporation of MNPs and LX within PCL microspheres was confirmed by both EDS and FTIR analysis. EDS analysis showed the presence of Iron in all formulations which is a confirmation of the successful encapsulation of MNPs in the microspheres. Also, the presence of Nitrogen in EDS spectra of F3 and F4 microspheres (Figures 7A and 7B) and its absence in the blank formulation F0 (Figure 7C) is a confirmation of the presence of LX in the F3 and F4 microspheres matrix. FTIR analysis confirmed the incorporation of MNPs within the microspheres as indicated by the band at 574.36 cm^{-1} present in F3 and F0 which is attributed to Fe–O stretching vibration. The additional bands at 1,647 and 1,533 cm^{-1} seen in the F3 spectrum but not in the F0 spectrum are attributed to the presence of LX in the F3 matrix, these bands correspond to C=O stretching and N–H bending vibration of LX, respectively[38]. The C=O is seen as a small shoulder due to the overlapping of the dominant C=O stretching of PCL at 1,721 cm^{-1}[44]. The presence of the characteristic bands for LX indicates that it is stable in the microspheres. It was also observed that the BET and BJH analysis of F3 results for surface area pore diameter and volume are in good agreement with previous reports that used the same method in the preparation of polymer microspheres[45].

The *in vitro* drug release profile of F3 showed a biphasic release; the initial higher release rate observed may be attributed to having drug molecules available at the surface or near the surface of the microspheres due to the presence of MNPs embedded in the bulk of the microspheres. This might have pushed the drug molecules nearer to the surface of the microspheres. The kinetics of drug release was studied using three mathematical models; zero-order, first-order,

and Higuchi to determine the most plausible release kinetics of LX from PCL microspheres. The initial fast release phase is best described by the Higuchi model. This model describes the drug release mechanism as a diffusion process based on Fick's law, which depends on the square root of time. Thus, this indicates that as the time of exposure to dissolution medium increases, the amount of drug released decreases. The reason behind this is that the drug is released initially from the surface region, which is the shortest diffusion path[46,47]. The second phase of drug release, the slower release phase is best described by first-order kinetics, which indicates that the amount of drug released is proportional at any time to the amount of drug remaining in the PCL microspheres[48].

Owing to the encapsulated superparamagnetic Fe_3O_4 nanoparticles, the microspheres exhibited superparamagnetic behavior as shown in Figure 4 which in turn allowed motion control via external magnetic fields. The cluster of microspheres is being pulled by a magnetic force according to $\mathbf{F}_B = (V\mathbf{M}\cdot\nabla)\mathbf{B}$, where $\mathbf{M}$ is the induced magnetization of the cluster, V is the volume, and $\mathbf{B}$ is the magnetic field. Further, ∇ is the gradient operator. Note that the magnetic force, at any given cluster position, depends on the magnetic moment and the gradient of the field. The magnetic force is balanced by the hydrodynamic drag force ($\mathbf{F}_d$) according to $\mathbf{F}_B + \mathbf{F}_d = 0$ assuming a sufficiently small mass and negligible gravitational and buoyancy forces[49]. The microsphere cluster shape remained intact during the journey along the predefined U-turn path indicating strong attractive forces between the individual microspheres. This would be due to the high M_s value associated with the 90 mg of MNPs used in F3. This in turn helps in efficient drug delivery with no significant microsphere or drug losses before reaching the desired location.

5. Conclusions

Encapsulation of LX together with MNPs in PCL microspheres was successfully achieved for the purpose of TDD. MNPs were added to magnetize the microspheres to enable their control via external magnetic fields. MNPs were first fabricated via the co-precipitation method. TEM images showed that MNPs were nearly spherical with a relatively narrow size distribution ranging between 20 and 50 nm. VSM results indicated their superparamagnetic behavior with high magnetization saturation (79.6 emu/g).

Several microsphere formulations were investigated in order to assess the effect of increasing the amount of MNPs, doubling the volume of the aqueous phase, and increasing the amount of the drug. All the microspheres showed smooth surfaces and had a size range between 800 and 2,000 nm. Increasing the amount of MNPs led to highly magnetized microspheres as expected while increasing the volume of the aqueous phase led to an improvement in microsphere separation as well as drug loading and encapsulation efficiency. Increasing the amount of drug from 50 to 80 mg, however, did not show an improvement in drug loading or encapsulation efficiency. The highest drug loading (10.7%) and encapsulation efficiency (83.90%) were observed for F3. The *in vitro* drug release profile was studied for F3, the results showed a biphasic release nature characterized by an initial high release rate followed by a steady slower release rate. Finally, open-loop control of the microspheres via external magnetic fields using a four coil planar system was conducted. A cluster of microspheres was successfully controlled to move in a U-shaped path indicating the potential of such microspheres to be used for targeted drug delivery. Future studies should be directed to the assessment of cytotoxicity of the prepared microspheres, the effect of applying an alternating magnetic field on the release profile of LX from the microspheres, and *in vivo* testing in rheumatoid arthritis-induced rat models. Closed loop control could also be applied in order to move drug carriers between specific locations without user intervention during the journey.

Acknowledgment

The authors would like to acknowledge the Institute of Analytical and Bioanalytical Chemistry, Ulm University for taking some of the SEM images presented in this work and also for performing the EDS analysis and BET analysis.

Author contributions

N.A.E.G: Conceptualization, methodology, investigation, data interpretation, validation, supervision, writing-original draft, writing—review, and editing.

A.M: Methodology, investigation, data interpretation, validation, writing—original draft

M.A.N: Investigation, data interpretation

R.Z: Investigation, data interpretation

L.E.Z: Investigation, data interpretation

I.K: Conceptualization, methodology, data interpretation, validation, supervision, writing—review and editing.

M.E.M: Conceptualization, methodology, data interpretation, validation, supervision, writing-original draft, writing—review and editing.

Disclosure statement

No potential conflict of interest was reported by the author(s). All authors gave final approval for publication and agree to be held accountable for the work performed therein.

ORCID

Nesrine Abdelrehim El Gohary http://orcid.org/0000-0001-6909-164X
Abdelrahman Mahmoud http://orcid.org/0000-0001-9907-9852
Mohamed Ashraf Nazmy http://orcid.org/0000-0003-4724-3133
Rami Zaabalawi http://orcid.org/0000-0002-3741-2733
Loaa El Zahar http://orcid.org/0000-0003-2768-4476
Islam S. M. Khalil http://orcid.org/0000-0003-0617-088X
Mohamed E. Mitwally http://orcid.org/0000-0001-8901-4967

References

[1] Helmy, H. S.; El-Sahar, A. E.; Sayed, R. H.; Shamma, R. N.; Salama, A. H.; Elbaz, E. M. Therapeutic Effects of Lornoxicam-Loaded Nanomicellar Formula in Experimental Models of Rheumatoid Arthritis. *Int. J. Nanomedicine.* **2017**, *12*, 7015–7023. DOI: 10.2147/IJN.S147738.

[2] Couvreur, P.; Barratt, G.; Fattal, E.; Vauthier, C. Nanocapsule Technology: A Review. *Crit. Rev. Therap. Drug Carrier Syst.* **2002**, *19*, 99–134. DOI: 10.1615/CritRevTherDrugCarrierSyst.v19.i2.10.

[3] Trivedi, R.; Kompella, U. B. Nanomicellar Formulations for Sustained Drug Delivery: Strategies and Underlying Principles. *Nanomedicine.* **2010**, *5*, 485–505. DOI: 10.2217/nnm.10.10.

[4] Zhang, X.; Xue, L.; Wang, J.; Liu, Q.; Liu, J.; Gao, Z.; Yang, W. Effects of Surface Modification on the Properties of Magnetic Nanoparticles/PLA Composite Drug Carriers and in Vitro Controlled Release Study. *Colloids Surf. A.* **2013**, *431*, 80–86. DOI: 10.1016/j.colsurfa.2013.04.021.

[5] Park, J.; Kim, J. Y.; Pané, S.; Nelson, B. J.; Choi, H. Acoustically Mediated Controlled Drug Release and Targeted Therapy with Degradable 3D Porous Magnetic Microrobots. *Adv. Healthcare Mater.* **2021**, *10*, 2001096. DOI: 10.1002/adhm.202001096.

[6] Singh, A. V.; Ansari, M. H. D.; Dayan, C. B.; Giltinan, J.; Wang, S.; Yu, Y.; Kishore, V.; Laux, P.; Luch, A.; Sitti, M. Multifunctional Magnetic Hairbot for Untethered Osteogenesis, Ultrasound Contrast Imaging and Drug Delivery. *Biomaterials.* **2019**, *219*, 119394. DOI: 10.1016/j.biomaterials.2019.119394.

[7] Pena-Francesch, A.; Giltinan, J.; Sitti, M. Multifunctional and Biodegradable Self-Propelled Protein Motors. *Nat. Commun.* **2019**, *10*, 1–10.

[8] Magdanz, V.; Khalil, I. S. M.; Simmchen, J.; Furtado, G. P.; Mohanty, S.; Gebauer, J.; Xu, H.; Klingner, A.; Aziz, A.; Medina-Sánchez, M. IRONSperm: Sperm-Templated Soft Magnetic Microrobots. *Sci. Adv.* **2020**, *6*, eaba5855. DOI: 10.1126/sciadv.aba5855.

[9] Saad, E. M.; El Gohary, N. A.; El-Shenawy, B. M.; Handoussa, H.; Klingner, A.; Elwi, M.; Hamed, Y.; Khalil, I. S.; El Nashar, R. M.; Mizaikoff, B. Fabrication of Magnetic Molecularly Imprinted Beaded Fibers for Rosmarinic Acid. *Nanomaterials.* **2020**, *10*, 1478. DOI: 10.3390/nano10081478.

[10] Tewabe, A.; Abate, A.; Tamrie, M.; Seyfu, A.; Siraj, E. A. Targeted Drug Delivery—from Magic Bullet to Nanomedicine: Principles, Challenges, and Future Perspectives. *J. Multidiscip. Healthc.* **2021**, *14*, 1711–1724. DOI: 10.2147/JMDH.S313968.

[11] Yang, J.; Park, S. B.; Yoon, H. G.; Huh, Y. M.; Haam, S. Preparation of Poly ε-Caprolactone Nanoparticles Containing Magnetite for Magnetic Drug Carrier. *Int. J. Pharm.* **2006**, *324*, 185–190. DOI: 10.1016/j.ijpharm.2006.06.029.

[12] Pietersz, G. A.; Wang, X.; Yap, M. L.; Lim, B.; Peter, K. Therapeutic Targeting in Nanomedicine: The Future Lies in Recombinant Antibodies. *Nanomedicine.* **2017**, *12*, 1873–1889. DOI: 10.2217/nnm-2017-0043.

[13] Cao, Z.; Li, D.; Wang, J.; Xiong, M.; Yang, X. Direct Nucleus-Targeted Drug Delivery Using Cascade pH_e/Photo Dual-Sensitive Polymeric Nanocarrier for Cancer Therapy. *Small.* **2019**, *15*, 1902022. DOI: 10.1002/smll.201902022.

[14] Amin, M.; Huang, W.; Seynhaeve, A. L.; Ten Hagen, T. L. Hyperthermia and Temperature-Sensitive Nanomaterials for Spatiotemporal Drug Delivery to Solid Tumors. *Pharmaceutics.* **2020**, *12*, 1007. DOI: 10.3390/pharmaceutics12111007.

[15] Saadat, M.; Manshadi, M. K.; Mohammadi, M.; Zare, M. J.; Zarei, M.; Kamali, R.; Sanati-Nezhad, A. Magnetic Particle Targeting for Diagnosis and Therapy of Lung Cancers. *J. Control. Release.* **2020**, *328*, 776–791. DOI: 10.1016/j.jconrel.2020.09.017.

[16] Chowdhury, S. M.; Lee, T.; Willmann, J. K. Ultrasound-Guided Drug Delivery in Cancer. *Ultrasonography* **2017**, *36*, 171–184. DOI: 10.14366/usg.17021.

[17] Linsley, C. S.; Wu, B. M. Recent Advances in Light-Responsive on-Demand Drug-Delivery Systems. *Ther. Deliv.* **2017**, *8*, 89–107. DOI: 10.4155/tde-2016-0060.

[18] Rossin, R.; Versteegen, R. M.; Wu, J.; Khasanov, A.; Wessels, H. J.; Steenbergen, E. J.; Ten Hoeve, W.; Janssen, H. M.; Van Onzen, A. H.; Hudson, P. J.; et al. Chemically Triggered Drug Release from an Antibody-Drug Conjugate Leads to Potent Antitumour Activity in Mice. *Nat. Commun.* **2018**, *9*, 1–11.

[19] Wang, J.; Xiong, Z.; Zheng, J.; Zhan, X.; Tang, J. Light-Driven Micro/Nanomotor for Promising Biomedical Tools: Principle, Challenge, and Prospect. *Acc. Chem. Res.* **2018**, *51*, 1957–1965. DOI: 10.1021/acs.accounts.8b00254.

[20] Lu, X.; Shen, H.; Zhao, K.; Wang, Z.; Peng, H.; Liu, W. Micro-/Nanomachines Driven by Ultrasonic Power Sources. *Chem. Asian J.* **2019**, *14*, 2406–2416. DOI: 10.1002/asia.201900281.

[21] Guo, J.; Gallegos, J. J.; Tom, A. R.; Fan, D. Electric-Field-Guided Precision Manipulation of Catalytic Nanomotors for Cargo Delivery and Powering Nanoelectromechanical Devices. *ACS Nano.* **2018**, *12*, 1179–1187. DOI: 10.1021/acsnano.7b06824.

[22] Chen, X. Z.; Hoop, M.; Mushtaq, F.; Siringil, E.; Hu, C.; Nelson, B. J.; Pané, S. Recent Developments in Magnetically Driven Micro-and Nanorobots. *Appl. Mater. Today.* **2017**, *9*, 37–48. DOI: 10.1016/j.apmt.2017.04.006.

[23] Hosney, A.; Abdalla, J.; Amin, I. S.; Hamdi, N.; Khalil, I. S. M. *In Vitro* Validation of Clearing Clogged Vessels Using Microrobots. Presented at the 6th IEEE International Conference on Biomedical Robotics and Biomechatronics (BioRob), Singapore, June 26–29, 2016.

[24] Niedert, E. E.; Bi, C.; Adam, G.; Lambert, E.; Solorio, L.; Goergen, C. J.; Cappelleri, D. J. A Tumbling Magnetic Microrobot System for Biomedical Applications. *Micromachines.* **2020**, *11*, 861. DOI: 10.3390/mi11090861.

[25] Kummer, M. P.; Abbott, J. J.; Kratochvil, B. E.; Borer, R.; Sengul, A.; Nelson, B. J. OctoMag: An Electromagnetic System for 5-DOF Wireless Micromanipulation. *IEEE Trans. Robot.* **2010**, *26*, 1006–1017. DOI: 10.1109/TRO.2010.2073030.

[26] El-Boubbou, K. Magnetic Iron Oxide Nanoparticles as Drug Carriers: Preparation, Conjugation and Delivery. *Nanomedicine.* **2018**, *13*, 929–952. DOI: 10.2217/nnm-2017-0320.

[27] Závišová, V.; Koneracká, M.; Štrbák, O.; Tomašovičová, N.; Kopčanský, P.; Timko, M.; Vavra, I. Encapsulation of Indomethacin in Magnetic Biodegradable Polymer Nanoparticles. *J. Magn. Magn. Mater.* **2007**, *311*, 379–382. DOI: 10.1016/j.jmmm.2006.11.177.

[28] Mhlanga, N.; Sinha Ray, S.; Lemmer, Y.; Wesley-Smith, J. Polylactide-Based Magnetic Spheres as Efficient Carriers for Anticancer Drug Delivery. *ACS Appl. Mater. Interfaces.* **2015**, *7*, 22692–22701. DOI: 10.1021/acsami.5b07567.

[29] Saravanan, M.; Bhaskar, K.; Maharajan, G.; Pillai, K. S. Ultrasonically Controlled Release and Targeted Delivery of Diclofenac Sodium via Gelatin Magnetic Microspheres. *Int. J. Pharm.* **2004**, *283*, 71–82. DOI: 10.1016/j.ijpharm.2004.06.023.

[30] Butoescu, N.; Seemayer, C. A.; Palmer, G.; Guerne, P. A.; Gabay, C.; Doelker, E.; Jordan, O. Magnetically Retainable Microparticles for Drug Delivery to the Joint: Efficacy Studies in an Antigen-Induced Arthritis Model in Mice. *Arthritis Res. Ther.* **2009**, *11*, R72. DOI: 10.1186/ar2701.

[31] Kim, H. J.; Lee, S. M.; Park, K. H.; Mun, C. H.; Park, Y. B.; Yoo, K. H. Drug-Loaded Gold/Iron/Gold Plasmonic Nanoparticles for Magnetic Targeted Chemo-Photothermal Treatment of Rheumatoid Arthritis. *Biomaterials.* **2015**, *61*, 95–102. DOI: 10.1016/j.biomaterials.2015.05.018.

[32] Usta, A.; Man, K. P.; Strong, N.; Misak, H.; Wooley, P. H.; Asmatulu, R. Investigating MTX-Loaded Magnetic Nanocomposite Particles for Treatment of Rheumatoid Arthritis. *J. Magn. Magn. Mater.* **2020**, *499*, 166171. DOI: 10.1016/j.jmmm.2019.166171.

[33] Agúndez, J. A.; Lucena, M. I.; Martínez, C.; Andrade, R. J.; Blanca, M.; Ayuso, P.; García-Martín, E. Assessment of Nonsteroidal Anti-Inflammatory Drug-Induced Hepatotoxicity. *Expert Opin. Drug Metab. Toxicol.* **2011**, *7*, 817–828. DOI: 10.1517/17425255.2011.574613.

[34] Liang, J.; Li, H.; Yan, J.; Hou, W. Demulsification of Oleic-Acid-Coated Magnetite Nanoparticles for Cyclohexane-in-Water Nanoemulsions. *Energy Fuels.* **2014**, *28*, 6172–6178. DOI: 10.1021/ef501169m.

[35] Yuanbi, Z.; Zumin, Q.; Huang, J. Preparation and Analysis of Fe3O4 Magnetic Nanoparticles Used as Targeted-Drug Carriers. *Chin. J. Chem. Eng.* **2008**, *16*, 451–455.

[36] Veiseh, O.; Gunn, J. W.; Zhang, M. Design and Fabrication of Magnetic Nanoparticles for Targeted Drug Delivery and Imaging. *Adv. Drug Deliv. Rev.* **2010**, *62*, 284–304. DOI: 10.1016/j.addr.2009.11.002.

[37] Kush, P.; Thakur, V.; Kumar, P. Formulation and in Vitro Evaluation of Propranolol Hydrochloride Loaded Polycaprolactone Microspheres. *Int. J. Pharm. Sci. Rev. Res.* **2013**, *20*, 282–290.

[38] He, Y.; Majid, K.; Maqbool, M.; Hussain, T.; Yousaf, A. M.; Khan, I. U.; Mehmood, Y.; Aleem, A.; Arshad, M. S.; Younus, A.; et al. Formulation and Characterization of Lornoxicam-Loaded Cellulosic-Microsponge Gel for Possible Applications in Arthritis. *Saudi Pharm. J.* **2020**, *28*, 994–1003. DOI: 10.1016/j.jsps.2020.06.021.

[39] Salviano, L. B.; Cardoso, T. M. D. S.; Silva, G. C.; Dantas, M. S. S.; Ferreira, A. D. M. Microstructural Assessment of Magnetite Nanoparticles (Fe3O4) Obtained by Chemical Precipitation under Different Synthesis Conditions. *Mat. Res.* **2018**, *21*, e20170764.

[40] Ibarra, J.; Melendres, J.; Almada, M.; Burboa, M. G.; Taboada, P.; Juárez, J.; Valdez, M. A. Synthesis and Characterization of Magnetite/PLGA/Chitosan Nanoparticles. *Mater. Res. Express* **2015**, *2*, 095010. DOI: 10.1088/2053-1591/2/9/095010.

[41] Cano, M.; Sbargoud, K.; Allard, E.; Larpent, C. Magnetic Separation of Fatty Acids with Iron Oxide Nanoparticles and Application to Extractive Deacidification of Vegetable Oils. *Green Chem.* **2012**, *14*, 1786–1795. DOI: 10.1039/c2gc35270b.

[42] Yeo, Y.; Park, K. Control of Encapsulation Efficiency and Initial Burst in Polymeric Microparticle Systems. *Arch. Pharm. Res.* **2004**, *27*, 1–12. DOI: 10.1007/BF02980037.

[43] Maravajhala, V.; Dasari, N.; Sepuri, A.; Joginapalli, S. Design and Evaluation of Niacin Microspheres. *Indian J. Pharm. Sci.* **2009**, *71*, 663–669. DOI: 10.4103/0250-474X.59549.

[44] Natarajan, V.; Krithica, N.; Madhan, B.; Sehgal, P. K. Formulation and Evaluation of Quercetin Polycaprolactone Microspheres for the Treatment of Rheumatoid Arthritis. *J. Pharm. Sci.* **2011**, *100*, 195–205. DOI: 10.1002/jps.22266.

[45] Mabrouk, M.; Bijukumar, D.; Mulla, J. A.; Chejara, D. R.; Badhe, R. V.; Choonara, Y. E.; Kumar, P.; du Toit, L. C.; Pillay, V. Enhancement of the Biomineralization and Cellular Adhesivity of Polycaprolactone-Based Hollow Porous Microspheres via Dopamine Bio-Activation for Tissue Engineering Applications. *Mater. Lett.* **2015**, *161*, 503–507. DOI: 10.1016/j.matlet.2015.08.146.

[46] Monteiro, M. S.; Lunz, J.; Sebastião, P. J.; Tavares, M. I. B. Evaluation of Nevirapine Release Kinetics from Polycaprolactone Hybrids. *Mater. Sci. Appl.* **2016**, *07*, 680–701.

[47] Dash, T. K.; Konkimalla, V. B. Poly-ϵ-Caprolactone Based Formulations for Drug Delivery and Tissue Engineering: A Review. *J. Control. Release.* **2012**, *158*, 15–33. DOI: 10.1016/j.jconrel.2011.09.064.

[48] Talevi, A.; Ruiz, M. E. Drug Release. In *The ADME Encyclopedia*. Cham: Springer, 2021.

[49] Barnsley, L. C.; Carugo, D.; Aron, M.; Stride, E. Understanding the Dynamics of Superparamagnetic Particles under the Influence of High Field Gradient Arrays. *Phys. Med. Biol.* **2017**, *62*, 2333–2360.